Spectroscopic Imaging Scanning Tunneling Microscopy as a Probe of Orbital Structures and Ordering

Wei-Cheng Lee[1] and Congjun Wu[1]

[1]*Department of Physics, University of California, San Diego, CA 92093*

Unlike charge and spin, the orbital degree of freedom of electrons in transition metal oxides is difficult to detect. We present the theoretical study of a new detection method in metallic orbitally active systems by analyzing the quasiparticle scattering interference (QPI) pattern of the spectroscopic imaging scanning tunneling spectroscopy, which is sensitive to orbital structures and orbital ordering. The QPIs for the d_{xz} and d_{yz}-orbital bands in the t_{2g}-orbital systems show a characteristic stripe-like feature as a consequence of their quasi-one-dimensional nature, which is robust against orbital hybridization. With the occurrence of orbital ordering proposed in $Sr_3Ru_2O_7$ and iron-pnictides, the stripe-like QPI patterns exhibit nematic distortion breaking the C_4-symmetry.

Orbital, a degree of freedom independent of charge and spin, plays an important role in various phenomena of transition metal oxides (d-orbital) and heavy-fermion compounds (f-orbital), including metal-insulator transitions, unconventional superconductivity, colossal magnetoresistance [1, 2, 3, 4]. Orbital ordering and excitations have been observed in many Mott-insulating transition metal oxides such as $La_{1-x}Sr_xMnO_3$, $La_4Ru_2O_{10}$, $LaTiO_3$, $YTiO_3$, $KCuF_3$, etc. [5, 6, 7, 8] In addition, cold atom optical lattices have opened up a new opportunity to study orbital physics with both bosons and fermions, which has recently attracted considerable experimental and theoretical research attentions[9, 10, 11, 12, 13, 14, 15].

Many metallic transition metal oxides, such as strontium ruthenates and iron pnictides, are orbitally active. Their Fermi surfaces are composed of different components of the t_{2g}-orbitals, *i.e.*, d_{xy}, d_{xz} and d_{yz}. Different from the d_{xy}-band which is quasi-two-dimensional (2D), the d_{xz} and d_{yz}-bands are quasi-one-dimensional with strong in-plane anisotropy. Their Fermi surfaces are strongly nested, resulting in strong incommensurate spin fluctuations in strontium ruthenates and iron pnictides [16, 17, 18]. Furthermore, the quasi-1D bands also play an important role in the electronic nematic ordering observed in the bilayer $Sr_3Ru_2O_7$ [19, 20, 21] between two consecutive metamagnetic transitions in the external magnetic field, which contributes another intriguing example of spin-orbital interplay [22, 23, 24, 25, 26]. The nematic ordering has been interpreted as orbital ordering between d_{xz} and d_{yz}-orbitals by us [27] and also independently by Raghu *et al.* [28].

In contrast to charge and spin whose detection methods have been maturely developed, the orbital degree of freedom is very difficult to measure especially in metallic orbital systems. In this letter, we present the theoretical study of a new method to detect the orbital degree of freedom by employing the technique of spectroscopic imaging scanning tunneling microscopy (SI-STM). This technique is an important tool to study competing orders

in strongly correlated systems [29, 30, 31, 32, 33], and has been just applied into the metallic t_{2g}-orbital systems of $Sr_3Ru_2O_7$ [34]. We find that this technique provides a sensitive method to detect orbital degree of freedom and orbital ordering by studying the quasi-particle interference (QPI) in the quasi-1D d_{xz} and d_{yz} bands. In contrast to the well-established QPI scenario for the single band system before, the T-matrix acquires momentum dependent form factors which forbid some QPI wavevectors and result in stripe features in the Fourier transformed STM images. The orbital ordering exhibits in the nematic distortion of the stripe QPI patterns. The applications of our analysis to the nematic orbital ordering in strontium ruthenates and the iron pnictide superconductors will be demonstrated.

We consider the band Hamiltonian with the d_{xz} and d_{yz}-orbital bands as: $H_0 = \sum_{\vec{k}\sigma} H_{\vec{k}\sigma}$, and

$$
\begin{aligned}
H_{\vec{k}\sigma} &= \epsilon_{xz,\vec{k}} d^\dagger_{xz\vec{k}\sigma} d_{xz,\vec{k}\sigma} + \epsilon_{yz,\vec{k}} d^\dagger_{yz,\vec{k}\sigma} d_{yz,\vec{k}\sigma} \\
&+ (f_{\vec{k}\sigma} d^\dagger_{xz,\vec{k}\sigma} d_{yz,\vec{k}\sigma} + h.c.),
\end{aligned}
\tag{1}
$$

where $\epsilon_{xz,\vec{k}} = -2t_\parallel \cos k_x - 2t_\perp \cos k_y - 4t' \cos k_x \cos k_y$, $\epsilon_{yz,\vec{k}} = -2t_\perp \cos k_x - 2t_\parallel \cos k_y - 4t' \cos k_x \cos k_y$. $f_{\vec{k}\sigma}$ is the hybridization between d_{xz} and d_{yz} orbitals, which is different from materials to materials and can be complex function in general. $t_\parallel$ and $t_\perp$ are the nearest neighbor longitudinal and transverse hopping integrals for the d_{xz} and d_{yz}-orbitals, and $t_\parallel >> t_\perp$. t' is the next-nearest neighbor intra-orbital hopping integral. We define the basis of the pseudo-spinor as $\hat{\phi}_{\vec{k}\sigma} = (d_{xz\vec{k}\sigma}, d_{yz\vec{k}\sigma})^T$. $H_{\vec{k}\sigma}$ can be diagonalized by introducing the unitary transformation $\hat{U}_{\vec{k}\sigma}$ such that $\hat{U}^\dagger_{\vec{k}\sigma} \hat{H}_{\vec{k}\sigma} \hat{U}_{\vec{k}\sigma} = \text{diag}\{E^+_{\vec{k}\sigma}, E^-_{\vec{k}\sigma}\}$. U reads in the basis of $\hat{\phi}_{\vec{k}\sigma}$ as

$$
\hat{U}_{\vec{k}\sigma} = \begin{pmatrix} \cos\theta_{\vec{k}\sigma} & -e^{i\delta_{\vec{k}\sigma}} \sin\theta_{\vec{k}\sigma} \\ e^{-i\delta_{\vec{k}\sigma}} \sin\theta_{\vec{k}\sigma} & \cos\theta_{\vec{k}\sigma} \end{pmatrix},
\tag{2}
$$

where $\tan 2\theta_{\vec{k}\sigma} = \frac{2|f_{\vec{k}\sigma}|}{\epsilon_{xz,\vec{k}} - \epsilon_{yz,\vec{k}}}$, $\delta_{\vec{k}\sigma} = \text{Arg}(f_{\vec{k},\sigma})$. The eigenvalues and the corresponding eigenvectors are:

$E^{\pm}_{\vec{k}\sigma} = (\epsilon_{xz,\vec{k}} + \epsilon_{yz,\vec{k}} \pm \sqrt{(\epsilon_{xz,\vec{k}} - \epsilon_{yz,\vec{k}})^2 + 4|f_{\vec{k}\sigma}|^2})/2$ and $\psi_{\vec{k}\sigma} = (\gamma_{+,\vec{k}\sigma}, \gamma_{-,\vec{k}\sigma})^T = \hat{U}^{\dagger}_{\vec{k}\sigma}\hat{\phi}_{\vec{k}\sigma}$, respectively.

Next we introduce the scattering Hamiltonian for the non-magnetic single impurity at $\vec{r}_i$. Assuming the isotropy of the impurity, H_{imp} does not mix d_{xz} and d_{yz} orbitals as $H_{imp} = V_0 \sum_{i\sigma} (d^{\dagger}_{xz,i\sigma}d_{xz,i\sigma} + d^{\dagger}_{yz,i\sigma}d_{yz,i\sigma})\delta_{i,\vec{r}_i}$, where we set the impurity location $\vec{r}_i = (0,0)$ at the origin. In the basis of the band eigen-function $\psi_{\vec{k}\sigma}$, H_{imp} is expressed as

$$H_{imp} = \frac{1}{N}\sum_{\vec{k},\vec{k}',\sigma} \hat{\psi}^{\dagger}_{\vec{k}\sigma,a} \hat{V}^{\sigma}_{\vec{k},\vec{k}';ab} \hat{\psi}_{\vec{k}'\sigma,b}, \quad (3)$$

where $\hat{V}^{\sigma}_{\vec{k},\vec{k}';ab} = V_0 \left[\hat{U}^{\dagger}_{\vec{k}\sigma}\hat{U}_{\vec{k}'\sigma}\right]_{ab}$ is the effective scattering matrix, and $a,b = \pm$ are eigen-band indices. This momentum-dependence generated by the orbital hybridization has non-trivial consequences in the QPI spectra shown later.

The Green functions with the impurity satisfy

$$\hat{G}_{\sigma}(\vec{k},\vec{k}') = \hat{G}_{0,\sigma}(\vec{k})\delta_{\vec{k},\vec{k}'} + \hat{G}_{0,\sigma}(\vec{k})\hat{T}^{\sigma}_{\vec{k},\vec{k}'}\hat{G}_{0,\sigma}(\vec{k}') \quad (4)$$

where $\hat{G}, \hat{G}_0$ and the T-matrix are 2×2-matrices in terms of band indices. The T-matrix and the bare Green's functions $\hat{G}_{0,\sigma}(\vec{k})$ defined as:

$$\hat{T}^{\sigma}_{\vec{k},\vec{k}'} = \hat{V}^{\sigma}_{\vec{k},\vec{k}'} + \frac{1}{N}\sum_{\vec{p}} \hat{V}^{\sigma}_{\vec{k},\vec{p}}\hat{G}_{0,\sigma}(\vec{p})\hat{T}^{\sigma}_{\vec{p},\vec{k}'}, \quad (5)$$

and $[\hat{G}^{-1}_{0,\sigma}(\vec{k})]_{ab} = (\omega + i\delta - E^a_{\vec{k}\sigma})\delta_{a,b}$.

In previous theoretical analysis of QPI [31], the single impurity T-matrix was simplified as momentum-independent for the single band systems. This simplification is no longer valid in hybridized quasi-1D bands of d_{xz} and d_{yz}. In the following, we consider a square lattice containing 41×41 sites and solve the momentum-dependent T-matrix numerically. The LDOS at energy E, which is proportional to the conductance (dI/dV) measured by the STM, and its Fourier transformation (FT-STM) can be calculated as

$$\rho(\vec{r},E) = -\frac{1}{N\pi}\sum_{\sigma,\vec{k},\vec{k}'} \text{Im}\{e^{-i(\vec{k}-\vec{k}')\cdot\vec{r}}$$
$$\times \text{Tr}\left[\hat{U}_{\vec{k},\sigma}\hat{G}_{\sigma}(\vec{k},\vec{k}',E)\hat{U}^{\dagger}_{\vec{k}',\sigma}\right]\},$$
$$\rho(\vec{q},E) = \frac{1}{N}\sum_{\vec{r}} e^{-i\vec{q}\cdot\vec{r}}\rho(\vec{r},E), \quad (6)$$

Note that in all the FT-STM images presented below, $\rho(\vec{q}=0,E)$ are removed to reveal the weaker QPI[31], and the absolute intensities of $\rho(\vec{q},E)$ are plotted.

We start with a heuristic example of ideal quasi-1D case in which only $t_{\parallel}$ is non-zero without hybridization. In this case, the Fermi surface of each band is a set of
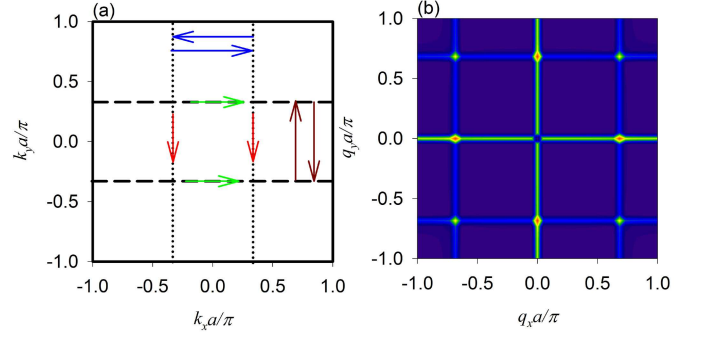

FIG. 1: (a) The Fermi surfaces with an ideal quasi-1D bands without hybridization and (b) the corresponding FT-STM image. The stripe features in (b) at $q_x = 0$ and $q_y = 0$ result from the quasiparticle scatterings indicated by arrows within the same lines in (a), and those appearing at $q_x = \pm2k_F$ and $q_y = \pm2k_F$ come from scatterings indicated by arrows between different lines in (a), echoing the Friedel oscillation in exact 1D case.

two straight lines located at $k_x = \pm k_F$ ($k_y = \pm k_F$) for d_{xz} (d_{yz}) bands as shown in the Fig. 1 (a). Because the DOS is uniform along the Fermi surface, all the quasiparticle scatterings on the Fermi surface are equally important. The quasiparticle scatterings occur either within the same 'Fermi lines' giving rise to the stripes on the $\hat{x}$ and $\hat{y}$ axes in the FT-STM image (Fig. 1(b)), or between the different 'Fermi lines' leading to the remaining weaker stripes in Fig. 1(b). These weaker stripes appearing at the lines of $q_x = \pm2k_F$ and $q_y = \pm2k_F$ are the quasi-1D analogues of Friedel oscillation in exact 1D systems. Note that all the QPIs have C_4 symmetry because we assume that the d_{xz} and d_{yz} bands are degenerate and no spontaneous nematic order is present.

With turning on the hybridization, naively it may be expected that these stripe features should disappear since the Fermi surfaces are 2D-like. However, we will show explicitly that due to the momentum-dependent T-matrix some quasiparticle scatterings on the Fermi surfaces are greatly suppressed even as the DOS of $\vec{k}$ points are large. As a result, the stripe features still survive as long as the Fermi surfaces remain connected. This unique feature distinguishes the hybridized quasi-1D bands from a single 2D band, for example, the d_{xy} band with similar Fermi surface topology.

Below we consider the on-site spin-orbit (SO) coupling $H_{SO} = \lambda \sum_i \vec{L}_i \cdot \vec{S}_i$ to hybridize the d_{xz} and d_{yz}-bands [28, 35]. Projecting it onto the d_{xz} and d_{yz}-subspace, we obtain the hybridization function as: $f_{\vec{k}\sigma} = i\sigma\lambda/2$. Consequently, the effective scattering matrix $\hat{V}^{\sigma}_{\vec{k},\vec{k}';ab}$ in the eigenband basis becomes:

$$\hat{V}^{\sigma}_{\vec{k},\vec{k}'} = V_0 \begin{bmatrix} \cos(\theta_{\vec{k}} - \theta_{\vec{k}'}) & -i\sigma\sin(\theta_{\vec{k}} - \theta_{\vec{k}'}) \\ i\sigma\sin(\theta_{\vec{k}} - \theta_{\vec{k}'}) & \cos(\theta_{\vec{k}} - \theta_{\vec{k}'}) \end{bmatrix}, \quad (7)$$

where $\tan 2\theta_{\vec{k}} = \lambda/(\epsilon_{xz,\vec{k}} - \epsilon_{yz,\vec{k}})$. The diagonal terms (the intra-band scattering) are modulated by the form factor of $\cos(\theta_{\vec{k}} - \theta_{\vec{k}'})$, which is suppressed around $\theta_{\vec{k}} - \theta_{\vec{k}'} \approx \pi/2$ is enhanced around $\theta_{\vec{k}} - \theta_{\vec{k}'} \approx 0$. For the aid to eyes, the values of the $\theta_{\vec{k}}$ are represented by the background gray scales plotted in Figs. 2(a),(c) and 3(a), showing white for $\theta_{\vec{k}} \to 0$ and dark gray for $\theta_{\vec{k}} \to \pi/2$. Since the larger $\hat{V}^{\sigma}_{\vec{k},\vec{k}'}$ leads to the larger $\hat{T}^{\sigma}_{\vec{k},\vec{k}'}$, the QPI wavevectors connecting two $\vec{k}$ points from different color areas have vanishing weights in the FT-STM images.

In the hybridized d_{xz} and d_{yz} bands, the DOS van Hove (vH) singularity occurs at $\vec{X} = (\pi, 0)$ and $\vec{X}' = (0, \pi)$. Fig. 2 summarizes the results for energies below and above the vH singularity. The model parameters are chosen as: $(t_{\parallel}, t_{\perp}, t', \lambda, V_0) = (1.0, 0.1, 0.025, 0.2, 1.0)$ consistent with those in Ref. [27, 28, 35]. In Fig. 2(b), the stripe features remain dominant in the FT-STM images at energy below the vH singularity as explained below. Although Fermi surface is a 2D closed loop shown in Fig. 2 (a), the QPI wavevectors corresponding to scatterings indicated by the solid arrows are prohibited due to the angular form factor discussed above. The dominant scatterings still occur in the same way as discussed in Fig. 1(a), except several $\vec{q}$ vectors on the stripes have stronger features because of the small variations of the DOS introduced by $t_{\perp}$ and t'. As energy crosses the vH singularity, the topology of the Fermi surface turns into discrete segments as shown in Fig. 2(c). The stripe features of the QPI wavevectors disappear and instead they become several discrete points whose positions depend on the model parameters. As the energy is very close to the vH singularity, it has been shown in Ref. [27, 28] that the spontaneous nematic order Δ appears with multi-band Hubbard interactions, which gives an anisotropic renormalization of dispersion of $\epsilon'_{xz,\vec{k}} = \epsilon_{xz,\vec{k}} + \Delta$ and $\epsilon'_{yz,\vec{k}} = \epsilon_{yz,\vec{k}} - \Delta$. Fig. 3 plots the Fermi surface and the FT-STM image for the ground state with $\Delta = 0.05$. The stripe features only extend along one particular direction and breaks the C_4 symmetry down to C_2 symmetry, as expected for a nematic order.

Now we connect the above discussion to the bilayer $Sr_3Ru_2O_7$ system which has the additional Fermi surfaces of the quasi-2D d_{xy}-band and the bilayer structure. The inter-band scatterings between the quasi-2D and 1D bands are also suppressed due to the similar reason of different orbital nature presented above. The QPI pattern of the intra d_{xy}-band scattering should follow the similar analysis published before [29, 31]. The quasi-1D bands of d_{xz} and d_{yz} have large bilayer splittings resulting in bonding and anti-bonding versions. Usually the impurity only lies in one layer, thus breaks the bilayer symmetry and induces both intra and inter-band scatterings among bonding and anti-bonding bands. And all of them should have the stripe pattern illustrated before.
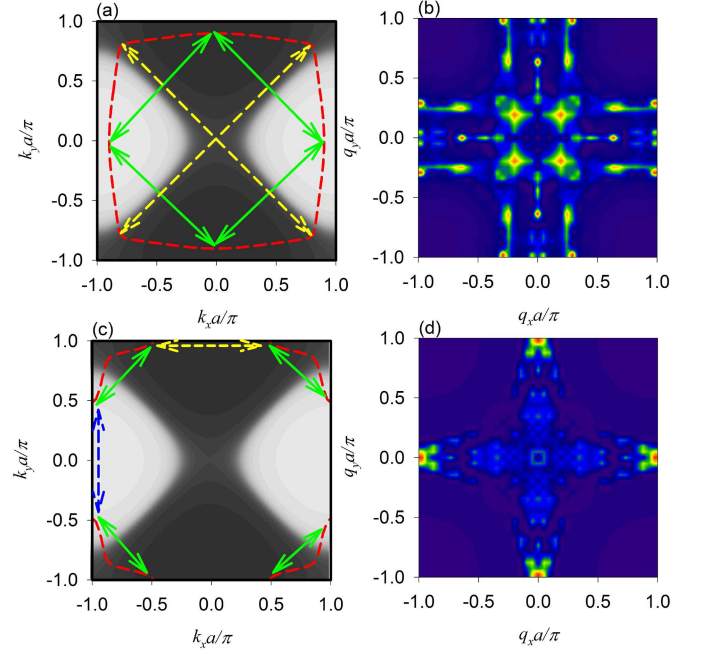

FIG. 2: Fermi surfaces (dashed lines) of the two quasi-1D bands at energies (a) just below the vH singularity ($E = 1.8$) and (c) just above the vH singularity ($E = 2.0$). The corresponding FT-STM images are presented in (b) and (d). The background gray scale in (a) and (c) represents the values of $\theta_{\vec{k}}$, exhibiting from white to dark gray for $\theta_{\vec{k}} = 0 \to \frac{\pi}{2}$. The scatterings between two $\vec{k}$ points in areas with different colors (indicated by the solid arrows) are strongly suppressed. The stripe pattern disappears and discrete QPI wavevector points become dominant when the Fermi surface breaks down to discrete segments. The dashed arrows in (a) and (c) refer to the scatterings responsible for the strongest features in the FT-STM images.

The change of the FT-STM images as energy across the vH singularity can be used to distinguish the orbital configuration of the Fermi surface responsible for the nematic ordering observed in $Sr_3Ru_3O_7$, which has been proposed both in the quasi-2D d_{xy}-band [22, 23, 24] and the quasi-1D bands of d_{xz} and d_{yz} [27, 28]. Both proposals have similar Fermi surface topology, but the QPIs will be very different. The stripe features are direct consequences of the quasi-1D bands which have comparable DOS on the Fermi surfaces. For the 2D d_{xy}-bands, the QPIs are dominated by several discrete $\vec{q}$ vectors connecting $\vec{k}$ points with largest DOS as has been demonstrated nicely in the high-T_c cuprate $Bi_2Sr_2CaCu_2O_{8+\delta}$[29]. Accordingly, we predict that if it is the 2D d_{xy}-band responsible for the nematic order, the FT-STM will show similar QPIs containing several discrete $\vec{q}$ vectors as the magnetic field is tuned through the critical point for the nematic order, while a significant change in the topologies of QPIs from Fig. 2(b)$\to$ Fig. 3(b)$\to$ Fig. 2(d) will be seen if the hybridized d_{xz} and d_{yz} bands are responsible.
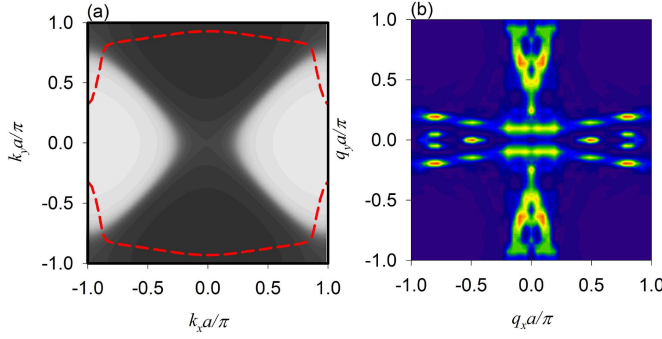
FIG. 3: (a) Fermi surface and (b) FT-STM image of the two quasi-1D band model for $Sr_3Ru_2O_7$ with nematic order right at the van Hove singularity ($E = 1.9$).

These results may also apply to the iron pnictide superconductors with multiple Fermi surface sheets: $\alpha_{1,2}$ bands located near the Γ point composed mostly of d_{xz} and d_{yz}-orbitals and $\beta_{1,2}$ bands residing near X and X' points with large fraction of d_{xy} orbital [36, 37]. Given that the tunneling rate along the $\hat{z}$ direction is strongly suppressed with the increase of magnitude of in-plane momentum $|\vec{k}_\parallel|$ [38], the tunneling matrix elements of $\beta_{1,2}$ bands are naturally to be much smaller than those of $\alpha_{1,2}$ bands. The similar suppression of tunneling matrix elements at large in-plane momentum has been demonstrated in the graphene systems [39]. As a result, SI-STM is expected to observe mostly the QPI scatterings from the $\alpha_{1,2}$ bands, and therefore the stripe features should be observed with a length roughly the size of the $\alpha_{1,2}$ pockets in the normal state of the iron pnictides. More interestingly, it has been suggested [40] based on a recent neutron scattering measurement performed on the undoped $CaFe_2As_2$ that a Heisenberg model with highly anisotropic in-plane exchange interactions is required to fit the spin-wave dispersion, indicating the possibility of nematic order [41]. Besides, the nematic order in LaOFeAs compound has also been theoretically predicted[18, 42, 43]. If such nematic order exists, the stripe features along one certain direction resembling Fig. 3(b) should be observable in the FT-STM image.

In conclusion, we have performed the theoretical investigation of a new detection method to the orbital degree of freedom and the orbital ordering in metallic transition metal oxides. For the quasi-1D d_{xz} and d_{yz} bands in the t_{2g}-orbital systems, the Fourier transformed STM image of the QPIs exhibit the stripe pattern. When the orbital hybridization is present, the T-matrix becomes momentum-dependent even for a single impurity problem and will suppress some QPI wavevectors depending on the hybridization angle $\theta_{\vec{k}}$. The consequences of the orbital ordering in $Sr_3Ru_2O_7$ and the iron pnictide superconductors have been pointed out as a nematic distortion of the stripe pattern of the QPI.

[1] M. Imada, A. Fujimori, and Y. Tokura, Rev. Mod. Phys. **70**, 1039 (1998).
[2] Y. Tokura and N. Nagaosa, Science **288**, 462 (2000).
[3] G. Khaliullin, Prog. Theor. Phys. Suppl. **160**, 155 (2005).
[4] D. I. Khomskii, Physica Scripta **72**, CC8 (2005).
[5] Y. Murakami *et al.*, Phys. Rev. Lett. **80**, 1932 (1998).
[6] C. Ulrich *et al.*, Phys. Rev. B **77**, 113102 (2008).
[7] H. Ichikawaa *et al.*, Physica B **281-282**, 482 (2000).
[8] P. Khalifah *et al.*, Science **297**, 2237 (2002).
[9] T. Müller *et al.*, Phys. Rev. Lett. **99**, 200405 (2007).
[10] W. V. Liu and C. Wu, Phys. Rev. A **74**, 13607 (2006).
[11] C. Wu *et al.*, Phys. Rev. Lett. **97**, 190406 (2006).
[12] C. Wu, Phys. Rev. Lett. **100**, 200406 (2008).
[13] C. Wu, Phys. Rev. Lett. **101**, 186807 (2008).
[14] C. Wu, Mod. Phys. Lett. B **23**, 1 (2009).
[15] W.-C. Lee, C. Wu, and S. Das Sarma, arXiv:0905.1146.
[16] A.P. Mackenzie and Y. Maeno, Rev. Mod. Phys. **75**, 657 (2003).
[17] I. Mazin and J. Schmalian, arXiv:0901.4790 (2009).
[18] H. Zhai, F. Wang, and D.-H. Lee, Phys. Rev. B **80**, 064517 (2009).
[19] S. A. Grigera *et al.*, Science **294**, 329 (2001).
[20] S. A. Grigera *et al.*, Science **306**, 1154 (2004).
[21] R. A. Borzi *et al.*, Science **315**, 214 (2007).
[22] H.-Y. Kee and Y. B. Kim, Phys. Rev. B **71**, 184402 (2005).
[23] C. Puetter, H. Doh, and H.-Y. Kee, Phys. Rev. B **76**, 235112 (2007).
[24] H. Yamase and A. Katanin, J. Phys. Soc. Japan **76**, 073706 (2007).
[25] A. Tamai *et al.*, Phys. Rev. Lett. **101**, 026407 (2008).
[26] J. F. Mercure *et al.*, arXiv:0902.3937 (2009).
[27] W.-C. Lee and C. Wu, Phys. Rev. B **80**, 104438 (2009).
[28] S. Raghu *et al.*, Phys. Rev. B **79**, 214402 (2009).
[29] Y. Kohsaka *et al.*, Nature **454**, 1072 (2008).
[30] T. Hanaguri *et al.*, Nature Physics **3**, 865 (2007).
[31] Q.-H. Wang and D.-H. Lee, Phys. Rev. B **67**, 020511 (2003).
[32] A. V. Balatsky, I. Vekhter, and J.-X. Zhu, Rev. Mod. Phys. **78**, 373 (2006).
[33] Y. Yin *et al.*, Phys. Rev. Lett. **102**, 097002 (2009).
[34] J. C. Davis, private communication.
[35] I. Eremin, D. Manske, and K. Bennemann, Phys. Rev. B **65**, 220502 (2002).
[36] K. Kuroki *et al.*, Phys. Rev. Lett. **101**, 087004 (2008).
[37] S. Graser *et al.*, New J. Phys. **11**, 025016 (2009).
[38] J. Tersoff and D. Hamann, Phys. Rev. Lett. **50**, 1998 (1983).
[39] Y. Zhang *et al.*, Nat. Phys. **4**, 627 (2008).
[40] J. Zhao *et al.*, Nature Phys. **5**, 555 (2009)
[41] R. R. Singh, arXiv:0903.4408 (2009).
[42] C. Fang *et al.*, Phys. Rev. B **77**, 224509(R) (2008).
[43] C. Xu *et al.*, Phys. Rev. B **78**, 020501 (2008).